SPEKTRA: Jurnal Fisika dan Aplikasinya
Volume 9, Issue 3, December 2024
Homepage: doi.org/10.21009/SPEKTRA

DOI: doi.org/10.21009/SPEKTRA.093.01

Laser-Assisted Scattering with Screened Diatomic Potential

Asmit Sapkota[1], Saddam Husain Dhobi[2,*], Subash Khatiwada[3]

[1]*Department of Physics, Goldengate International College, Tribhuvan University, Battisputali, Kathmandu 44600, Nepal*
[2]*Central Department of Physics, Tribhuvan University, Kirtipur 44618, Kathmandu, Nepal*
[3]*Department of Physics, St. Xavier's College, Tribhuvan University, Maitighar, Kathmandu 44600, Nepal*

*Corresponding Author Email: saddam@ran.edu.np

Received: 29 July 2024
Revised: 25 October 2024
Accepted: 8 November 2024
Online: 19 November 2024
Published: 30 December 2024

SPEKTRA: Jurnal Fisika dan Aplikasinya
p-ISSN: 2541-3384
e-ISSN: 2541-3392

ABSTRACT

This study explores the differential cross section (DCS) for laser-assisted scattering of diatomic molecules, considering various polarization conditions (linear, circular, elliptical) and potential parameters. The primary objective is to understand how polarization, screening effects, and potential parameters influence the scattering behavior. Utilizing a model that incorporates the Morse potential with screening effects, the analysis treats the laser field classically as a time-dependent, spatially homogeneous electric field, while the electron dynamics are described quantum mechanically using the Schrödinger equation. The Volkov wavefunction is derived, and the first-Born S-matrix element is computed to evaluate the scattering process. The results show that the DCS decreases with increasing screening parameters, with linear polarization yielding higher values than circular or elliptical polarization. Specifically, at an initial momentum of 8 MeV and a final momentum of 9 MeV, the DCS for elliptical polarization is notably higher. The DCS also varies with potential strength and well width, showing a peak at 0.14 Å for potential well width. The findings suggest that linear polarization is most effective for scattering studies under varying potential strengths. It is recommended to focus on linear polarization for enhanced scattering efficiency and to carefully adjust screening parameters and potential well widths for optimal results.

Keywords: differential cross section, laser-assisted scattering, polarization conditions, morse potential, screening effects

INTRODUCTION

Laser technology has experienced significant advancements in intensity, frequency, and time domain capabilities in the last two decades. These improvements have led to the discovery of highly nonlinear laser-induced phenomena such as above-threshold ionization (ATI) and high-order harmonic generation. Additionally, well-known processes have been modified by the presence of intense laser pulses. While the dynamic aspects of the ionization of atoms in a strong laser field are now well understood, theoretical analysis of similar processes in more complex targets, such as diatomic and polyatomic molecules, remains an active area of research. Recent experiments have shown that molecules behave differently in intense laser fields compared to weak field conditions, with new phenomena such as Coulomb explosion, bond softening, vibrational trapping, optically triggered explosions, and above-threshold dissociation being observed. Even the simplest process, multiphoton sequential ionization, exhibits many new features compared to atomic ionization. Understanding the ionization mechanism and its properties is crucial, as ionization is often followed by interesting secondary processes such as fragmentation or rescattering of the photoelectron [1]. Diatomic molecules subjected to strong laser pulses exhibit a wide range of fundamentally important processes influenced by the laser pulse parameters and the properties of the diatomics. Varró et al. [2] presented a general mathematical procedure to handle interactions described by a Morse potential in the presence of strong harmonic excitation, accounting for permanent and field-induced terms and their gradients in the dipole moment function. Their analytic formulae for bond-length change and shifted energy eigenvalues of vibrations provide insights into the behavior of H_2 and LiH when driven by near- or mid-infrared lasers at intensities around 10^{13} W cm^{-2}.

The change in internuclear distance caused by a laser pulse significantly influences the attosecond streaking spectrum and the formation of vibrational wave packets in diatomic molecules. Wei et al. [3] explored the photoelectron momentum distributions of H_2 and N_2, and their companion atoms Ar and Xe, under close-to-circularly polarized laser fields. They observed significant deviations in the results for N_2 compared to Xe, attributing these differences to the two-center interference effect in diatomic molecules, which varies due to the parity difference in their molecular ground-state wave functions. Despite the established theoretical framework for molecules interacting with laser fields, analytic results in the strong-field domain are rare and often approximate, while numerical methods can be computationally expensive for infrared wavelengths. Therefore, developing new analytic methods for molecules in strong fields is of great significance. Recent studies using fully quantized approaches have shown that intense laser-atom interactions can generate controllable high-photon-number entangled coherent states and coherent state superpositions, revealing new phenomena not observable within semiclassical theories. Stammer et al. [4] provided a comprehensive fully quantized description of intense laser-atom interactions, discussing processes such as high-harmonic generation and above-threshold ionization, and their implications for quantum state engineering of light.

Laser-driven nuclear dynamics of diatomic molecules have been investigated extensively, although many studies often neglect field-induced terms of the dipole moment function.

Corkum's [5] well-known three-step model has played a crucial role in the development of ultrashort pulse generation techniques, which are essential for attosecond science. Attosecond bursts of light, with durations shorter than a femtosecond, have enabled researchers to study electron dynamics in atoms and molecules on their natural timescales, facilitating the control of chemical reactions at the electronic level and obtaining time-resolved images of electronic motion. Palacios et al. [6] provided an overview of theoretical tools capable of describing electron and nuclear dynamics resulting from interactions with femto- and attosecond UV/XUV radiation, highlighting the time-dependent Feshbach close-coupling (TDFCC) formalism used to investigate various attosecond phenomena in the hydrogen molecule.

Most theoretical approaches to date have explored H_2 using the fixed nuclei approximation (FNA), with only a few considering both electronic and nuclear degrees of freedom while ignoring the dependence of electronic structure on internuclear distance. However, some implementations within the FNA have achieved significant breakthroughs, such as the first successful descriptions of one-photon and two-photon double ionization of H_2 [7]. The advancement of laser technology has revitalized the research field of optics, allowing for more detailed information to be obtained. Yadav et al. [8] developed a mathematical model to calculate differential cross sections in the presence of a Coulomb potential and an elliptically polarized beam with single photon absorption. Their model demonstrated that the differential cross section increases with wavelength and decreases with electron energy under elliptically polarized beams, reaching a maximum at a 1.56 radian polarized angle. Dhobi et al. [9] studied the differential cross-section in the presence of a weak laser field during inelastic scattering, finding that the cross-section increases when the target absorbs energy and varies with the scattering angle.

Dhobi et al. [10] also investigated the thermodynamic properties of thermal electrons participating in scattering events in the presence of a laser field, using a thermal Hamiltonian model. They found that thermodynamic energy around the target exhibits destructive interference at certain field amplitudes and temperatures, with the thermal Hamiltonian resembling a Coulomb potential. Further studies by Dhobi et al. [11] on laser-assisted thermal electron-hydrogen atom elastic scattering revealed that differential cross-sections vary with scattering angles and incidence energies, highlighting the differences between thermal and nonthermal electrons in the presence of a laser field.

The literature on laser-induced phenomena in diatomic molecules has made significant progress in understanding processes like above-threshold ionization, high-order harmonic generation, and multiphoton sequential ionization. However, a notable research gap exists concerning the study of DCS involving a Morse potential in the presence of a laser field. While Varró et al. [2] developed a mathematical procedure for interactions described by a Morse potential under strong harmonic excitation and applied their results to H2 and LiH, they did not investigate DCS with laser fields or consider the screening effect. Moreover, existing studies often neglect field-induced terms in the dipole moment function or rely on fixed nuclei approximations, leaving the complex interplay between molecular structure, electronic wave function symmetry, and laser fields insufficiently explored. Therefore, this work aims to address this gap by studying the DCS with a laser field and a screening Morse potential,

providing new insights into the behavior of diatomic molecules under intense laser fields and contributing to a more comprehensive understanding of laser-molecule interactions.

The introduction effectively sets the stage for the research by highlighting advancements in laser technology and their impact on nonlinear laser-induced phenomena. It emphasizes the need for further exploration of diatomic molecules in strong laser fields, particularly regarding DCS and interactions with a screening Morse potential, filling a notable gap in existing research.

METHODS AND MATERIALS

To study the DCS, we use a model that incorporates the Morse potential with screening parameters under laser-assisted scattering. This approach allows us to analyze the interactions between diatomic molecules and laser fields, considering both the screening effects and the dynamic changes in molecular structure induced by the laser. The vector potential is treated as spatially homogeneous and time-dependent. In our calculations, the collision dynamics are treated quantum mechanically, while the laser field is treated classically as a single-mode, spatially homogeneous electric field. We work in the Coulomb gauge, with the vector potential of a field propagating along the z-axis and represented in the collision plane. This model aims to provide a deeper understanding of the complex interplay between molecular geometry, electronic wave function symmetry, and intense laser fields.

$$A(t) = A_0\hat{x}\cos(\omega t + \phi) + A_0\hat{y}\sin(\omega t + \phi)\tan\left(\frac{\eta}{2}\right). \quad (1)$$

This describes the vector potential A(t) of the laser field. The vector potential is crucial in laser-matter interactions, as it describes the momentum transferred from the electromagnetic field to the charged particles (such as electrons in the molecule). Here, the laser field is expressed in terms of two components along the x- and y-axes. A_0 represents the amplitude of the vector potential, ω is the angular frequency of the laser., ϕ is the phase of the laser field and the term tan(η/2) introduces an angle η, likely relating to the ellipticity of the polarization of the laser field. The corresponding electric field E(t) associated with the vector potential. The electric field is directly responsible for driving the dynamics of charged particles, such as electrons in a molecule, causing phenomena like ionization, excitation, or dissociation.

$$E(t) = E_0\hat{x}\sin(\omega t + \phi) - E_0\hat{y}\cos(\omega t + \phi)\tan\left(\frac{\eta}{2}\right). \quad (2)$$

Here, E_0 is the electric field amplitude, proportional to the time derivative of the vector potential. The electric field components along the x- and y-axes are again modulated by the cosine and sine functions of (ωt+ϕ), corresponding to the time evolution of the laser field. The η measures the degree of ellipticity of the field, with $\eta = 0$ corresponding to linear polarization and $\eta = \pi/2$ to circular polarization. $E_0 = \frac{\omega A_0}{c}$ and ω represent the peak electric field strength and the laser angular frequency, respectively. We start by obtaining the wavefunction of a free electron in the presence of a laser field, where its non-relativistic motion is described by the Schrödinger equation.

$$i\frac{\partial}{\partial t}\psi(r,t) = H_L\psi(r,t) = \frac{1}{2}\left(p^2 + \frac{A(t)}{c}\right)\psi(r,t) \quad (3)$$

The solve of EQUATION (3) give give the Volkov wavefunction [12],

$$\chi_k(r,t) = \left(\frac{2\pi}{V}\right)^{-\frac{3}{2}} \exp[i(k\cdot r - E_k t - R_k \sin(\omega t - \gamma_k))] \qquad (4)$$

Where, $R_k = \alpha_0((k\cdot\hat{x})^2 + (k\cdot\hat{y})^2)\tan^2\left(\frac{\eta}{2}\right)$, and $\tan(\gamma_k) = \frac{k\cdot\hat{y}}{k\cdot\hat{x}}\tan\left(\frac{\eta}{2}\right)$, $\alpha_0 = \frac{E_0}{\omega^2}$ the amplitude associated with the classical quiver motion of the electron in the laser field is denoted by the amplitude term, and its kinetic energy is given by E_k=k^2/2. In the Volkov solution, as shown in EQUATION (4), the A^2 term is omitted, as it can be removed from the Schrödinger Equation, EQUATION (3), by a unitary transformation. The Volkov wave function in EQUATION (4) is normalized to a δ function.

$$\chi_k(r,t) = (2\pi)^{-\frac{2}{3}} \exp\left[i\left(k\cdot r - E_k t - \alpha_0((k\cdot\hat{x})^2 + (k\cdot\hat{y})^2)\tan^2\left(\frac{\eta}{2}\right)\sin(\omega t - \gamma_k)\right)\right] \qquad (5)$$

The central quantity to be evaluated is therefore the direct first-Born S-matrix element [13-14], we have

$$S_{B1} = -i\int_{\infty}^{\infty} dt \left\langle \chi_{k_f}|V|\chi_{k_i}\right\rangle \qquad (6)$$

Now putting the value of $\chi_{k_f}(r,t)$ and $\chi_{k_i}(r,t)$ are final and initial wave function of electron in laser field and $V = \left[De^{-2a(r+R_0)} - 2e^{-a(r+R_0)}\right]e^{-\eta r}$ is morse screening potential [2]. The Morse potential function, introduced by Philip Morse in 1929 [15], is a three-parameter empirical model for potential energy. It is useful for modeling the interaction between atoms in a diatomic molecule and between an atom and a surface. Unlike the Harmonic potential, the Morse potential accounts for dissociation, which enhances its applicability. The formula for the Morse potential as $V=D_e[1-2e^{-\alpha(r-R_0)}+ e^{-2\alpha(r-R_0)}]$ [16-19]. This is new potential decrease for this study and hence putting the value from (5) in (6) of $\chi_{k_f}(r,t)$ and $\chi_{k_i}(r,t)$ as well as potential we have from EQUATION (5);

$$\begin{aligned} S_{B1} &= -i(2\pi)^{-\frac{4}{3}}\left[\times\int_{-\infty}^{+\infty} dt \exp\left[iR_{k_f}\sin\left(\omega t - \gamma_{k_f}\right) - R_{k_i}\sin\left(\omega t - \gamma_{k_i}\right)\right]t\right] \\ &\times\left[D\int_0^{2\pi} d\phi\int_0^{\pi} sin\theta\, d\theta\int_0^{\infty} r^2 dr\; e^{-2ar-2aR_0-iqrcos\theta-\eta r}\right. \\ &\left. -\int_0^{2\pi} d\phi\int_0^{\pi} sin\theta\, d\theta\int_0^{\infty} 2r^2 dr\; e^{-ar-aR_0-iqrcos\theta-\eta r}\right] \end{aligned} \qquad (7)$$

On Integrate this EQUATION (7) and we get

$$S_{B1} = -\frac{i}{2\pi}\sum_{m,n=-\infty}^{\infty} J_m\left(R_{k_f}\right)J_n\left(R_{k_i}\right)\, e^{i(m\gamma_f - n\gamma_i)} \times\left[\frac{4\pi D e^{-2aR_0}(2a+\eta)}{(q^2+(2a+\eta)^2)^2} - \frac{16\pi e^{-2aR_0}(2a+\eta)}{(q^2+(2a+\eta)^2)^2}\right] \quad (8)$$

Now T-matrix is obtained as

$$T = -\frac{i}{2\pi}\sum_{m,n=-\infty}^{\infty} J_m\left(R_{k_f}\right)J_n\left(R_{k_i}\right)\, e^{i(m\gamma_f - n\gamma_i)} \times\left[\frac{4\pi D e^{-2aR_0}(2a+\eta)}{(q^2+(2a+\eta)^2)^2} - \frac{16\pi e^{-2aR_0}(2a+\eta)}{(q^2+(2a+\eta)^2)^2}\right] \quad (9)$$

Also, the DCS is obtained as

$$\frac{d\sigma}{d\Omega} = \frac{k_f}{ki}|T|^2 \quad (10)$$

$$\frac{d\sigma}{d\Omega} = \frac{k_f}{ki}\left|-\frac{i}{2\pi}\sum_{m,n=-\infty}^{\infty} J_m\left(R_{k_f}\right)J_n\left(R_{k_i}\right)\, e^{i(m\gamma_f - n\gamma_i)} \times\left[\frac{4\pi D e^{-2aR_0}(2a+\eta)}{(q^2+(2a+\eta)^2)^2} - \frac{16\pi e^{-2aR_0}(2a+\eta)}{(q^2+(2a+\eta)^2)^2}\right]\right|^2 \quad (11)$$

RESULT AND DISCUSSION

The ingestion of DCS for a scattering process under various polarization conditions (linear, circular, elliptical) as a function of screening parameters. The initial and final momenta were set at 8 MeV and 9 MeV, respectively. The analysis included Bessel function parameters and ellipticity values (0, π/2, π), with screening parameters ranging from 0 to 1. The interaction potential was defined by potential strength and width, both set to 1. The DCS for each polarization state against the screening parameter, thus illustrating the variations in scattering behavior with different polarizations and screening effects, in FIGURE 1. The results indicate that the DCS decreases with increasing screening parameters. Notably, the DCS for linear and circular polarizations remains nearly identical, whereas the DCS for elliptical polarization is observed to be higher. This behavior can be attributed to the nature of the interaction between the projected and target particles, influenced by the screening parameters.

In the lower region of screening parameters, the DCS is significantly higher as shown in FIGURE 1. This can be explained by the prominent role of the Coulomb effect between the projectile and the bound electron when the screening is low. The screening parameter moderates the interaction potential, and at low values, the Coulomb interaction is more

pronounced, leading to higher DCS values. Conversely, as the screening parameter increases, the DCS decreases. This reduction is because the higher screening effectively weakens the Coulomb interaction between the projectile and the bound electron, thus lowering the DCS. In this scenario, the interaction between the screening electron and the projected electron is more influential, while the impact of the bound electron's Coulomb interaction becomes negligible. When comparing the different polarization states, the DCS for elliptical polarization is higher than that for linear polarization, particularly in the context of the screening effect. The screening electron, positioned between two diatomic atoms, contributes to this discrepancy. The enhanced interaction due to the elliptical polarization leads to a higher DCS compared to the linear polarization case. The circular polarization shows similar DCS values to the linear case, suggesting that the nature of the interaction does not significantly change between these two polarization states under the given conditions.

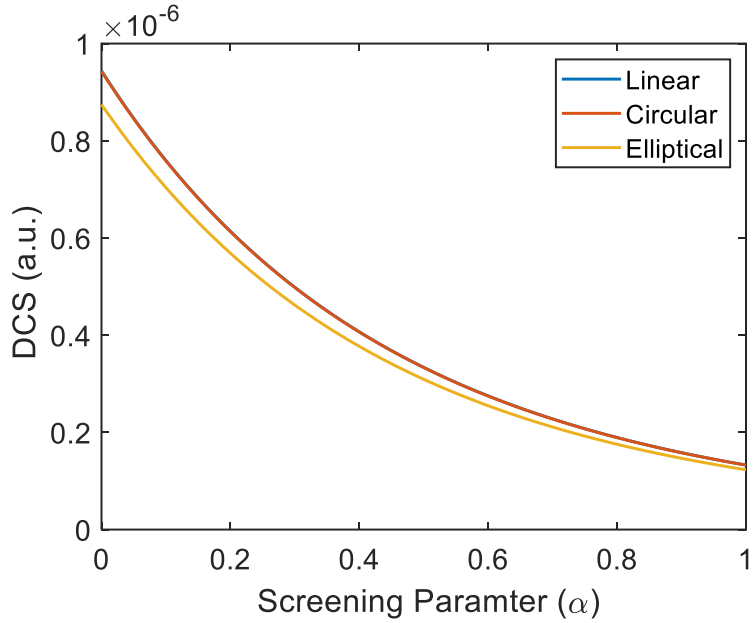

FIGURE 1. DCS with Screening parameters for linear, circular and elliptical.

The analysis highlights the critical influence of screening parameters and polarization states on the scattering process. The screening effect plays a pivotal role in modulating the interaction potential, which in turn affects the DCS as shown in FIGURE 1. Understanding these dependencies is crucial for interpreting scattering phenomena in various physical contexts, particularly in scenarios involving intense laser fields and complex molecular interactions. Electron screening for nuclear reactions in metals plays an unexpected and important role in enhancing reaction cross sections in the ultra-low energy region [20]. The screening effect of the atomic electrons plays an important role in the cross section itself, as well as in the radiation power spectrum [21-22].

The DCS for a scattering process under different polarization conditions (linear, circular, elliptical) as a function of initial momentum, with a fixed final momentum of 9 MeV. The study employs first-order Bessel functions, ellipticity values of 0, π/2, and π, and a screening

parameter of 0.1. The potential parameters are set to a strength of 1 and a potential well of 1. The DCS for each polarization state is computed and plotted against the initial momentum, as illustrated in FIGURE 2, to show how scattering behavior varies with different polarizations and momentum changes. Similar behavior of the DCS is observed for other screening parameters, potential well depths, and strengths, but with different amplitudes. FIGURE 2 demonstrates that the DCS increases with initial momentum starting from 8 MeV, converges at a certain point DCS 10^{-6} a.u, and then diverges again, showing distinct patterns for different polarizations. The converges DCS about 10^{-6} a.u. shows that all case of polarization has same affect and has same DCS. The DCS for linear polarization case increase with energy and become maximum up to 1.5 x 10^{-6} a.u. while for circular and elliptical maximum DCS observed up to 10^{-6} a.u. and then after this decrease and become minimum. It is observed that the DCS for linear polarization is higher than for circular and elliptical polarizations. A significant fluctuation in the DCS is noted in the energy range of 8 to 11 MeV. This fluctuation is attributed to the effect of the screening parameters.

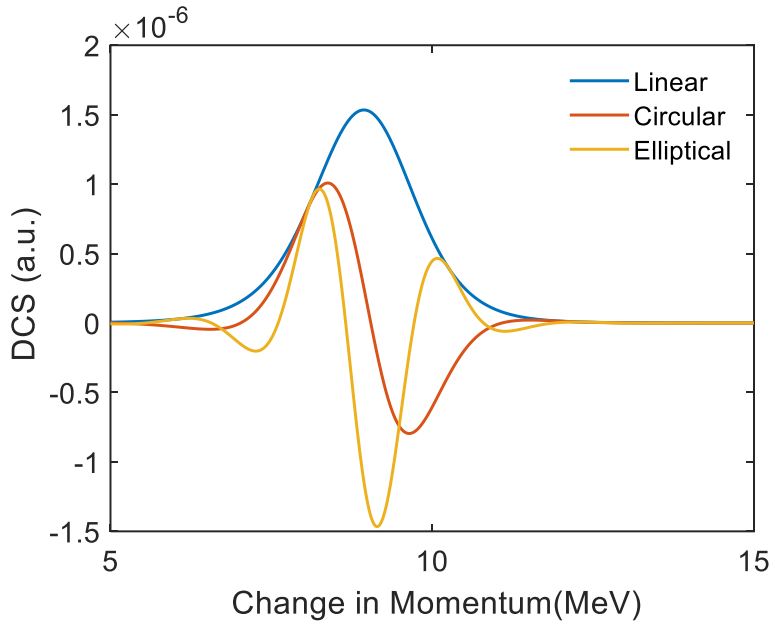

FIGURE 2. DCS with change in momentum for linear, circular and elliptical.

In the initial momentum range of 8 to 11 MeV, the DCS decreases due to the influence of the Bessel function. After reaching 11 MeV, the DCS stabilizes and remains almost constant as shown in FIGURE 2. This behavior can be understood by considering the screening effect in the context of diatomic molecules. Below 8 MeV, the diatomic molecules act as a single spherical atom because the screening parameter has a negligible effect. In this range, the atom appears as a single target, and the interaction primarily involves the Coulomb force between the projectile and the bound electrons. However, in the momentum range of 8 to 11 MeV, the screening effect becomes more significant, causing high fluctuations in the DCS. This is because the interaction now includes both the projectile electron and the screening electron. The screening effect modulates the Coulomb interaction, making it more complex and

resulting in fluctuations in the DCS. This indicates that the screening electron starts playing a crucial role, interacting with the projectile electron while the effect of the atom is minimized.

After 11 MeV, the DCS becomes almost constant as shown in FIGURE 2, indicating a balance in the interaction forces. This implies that the screening effect reaches a saturation point, and the dominant interactions are between the projectile and the screening electrons, with minimal influence from the atomic structure itself. The results suggest that by manipulating the screening parameters, one can study and control the impact of DCS effectively. The screening effect can be leveraged to tailor the DCS according to specific requirements, providing a powerful tool for controlling scattering processes in various applications. This study highlights the importance of considering both the initial momentum and the screening parameters to understand the scattering behavior comprehensively and to achieve desired outcomes in practical scenarios. Bartschat et al. [23] study quantum-mechanical calculations of cross sections for electron collisions with atoms and molecules and found the cross section increase with energy and become maximum and then decrease in absence of laser field. Similary different authors also found same nature with different atom [24-26]

The DCS for a scattering process under different polarization conditions—linear, circular, and elliptical—as a function of potential strength (D), with the initial and final momenta set to 9.1 MeV and 9 MeV, respectively. The calculations employ first-order Bessel functions, a screening parameter of 0.1, and a potential width of 1. FIGURE 3 illustrates how the DCS varies with potential strength D for each polarization state, providing insights into how scattering behavior is influenced by different polarizations and potential strengths. FIGURE 3 reveals that the DCS initially decreases as the potential strength increases, reaching a minimum value at 4 eV. Beyond this point, the DCS begins to rise with increasing potential strength. This trend indicates a complex relationship between the potential strength and the scattering cross-section.

For linear polarization, the DCS shows a clear and significant response to changes in potential strength. The initial decrease in DCS with increasing suggests that a stronger potential initially reduces the scattering efficiency. However, as the potential strength continues to increase, the DCS starts to rise, indicating that the scattering process becomes more favorable under higher potential strengths. This behavior underscores the effectiveness of linear polarization in diatomic molecules when varying the potential strength, highlighting its importance in practical applications where potential control is crucial. Conversely, the DCS for circular and elliptical polarizations exhibits negative values across the range of potential strengths. These negative values are non-physical and indicate that circular and elliptical polarizations are ineffective for the given scattering conditions. This lack of physical significance suggests that these polarizations do not provide meaningful results in the context of varying potential strength and diatomic interactions under the specified parameters.

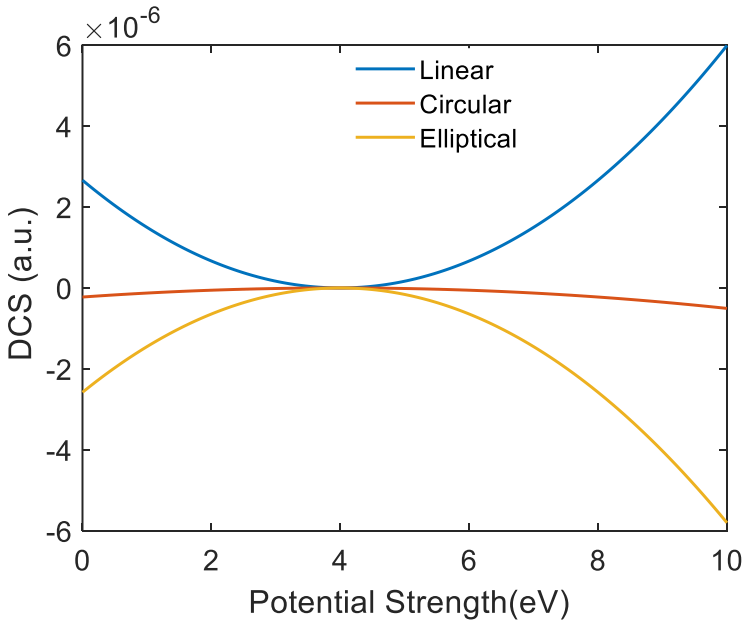

FIGURE 3. DCS with Potential strength for linear, circular and elliptical.

The findings demonstrate that linear polarization is the most effective polarization condition for studying scattering processes with varying potential strengths in diatomic molecules. The clear and physically meaningful DCS behavior observed with linear polarization contrasts with the non-physical results for circular and elliptical polarizations. This outcome emphasizes the need to carefully choose the polarization condition in scattering experiments and applications, as the choice significantly impacts the interpretability and usefulness of the results.

The analysis of DCS for a scattering process under various polarization conditions—linear, circular, and elliptical—as a function of the potential well width. The study uses initial and final momenta set to 10.1 MeV and 9 MeV, respectively, with first-order Bessel functions, screening parameter of 0.1, and a fixed potential strength of 1. The potential well width is varied from 0 to 1, and the DCS is calculated and plotted against this parameter. FIGURE 4 illustrates how scattering behavior changes with different polarizations and varying potential well widths. FIGURE 4 shows that the DCS for linear and elliptical polarizations increases with the potential well width, while the circular polarization does not exhibit a significant response in this range. The DCS values for linear and elliptical polarizations demonstrate a pronounced increase with smaller potential well widths, reaching a maximum at 0.14 Å. Beyond this width, the DCS decreases and eventually stabilizes. This decrease can be attributed to the effects of the Bessel function, which influences the scattering dynamics as the potential well width becomes larger.

The increase in DCS with smaller potential well widths for both linear and elliptical polarizations indicates that the scattering efficiency improves as the well width is reduced. The maximum DCS observed at 0.14 Å suggests an optimal potential well width for enhanced scattering under these polarization conditions. This result is particularly relevant for applications where maximizing the scattering cross-section is critical. For circular

polarization, the DCS does not show a meaningful variation with the potential well width, indicating that this polarization condition may not be effective for probing scattering processes in this context. The lack of significant results for circular polarization suggests that it may not be suitable for studies involving changes in the potential well width for diatomic molecules under the given parameters.

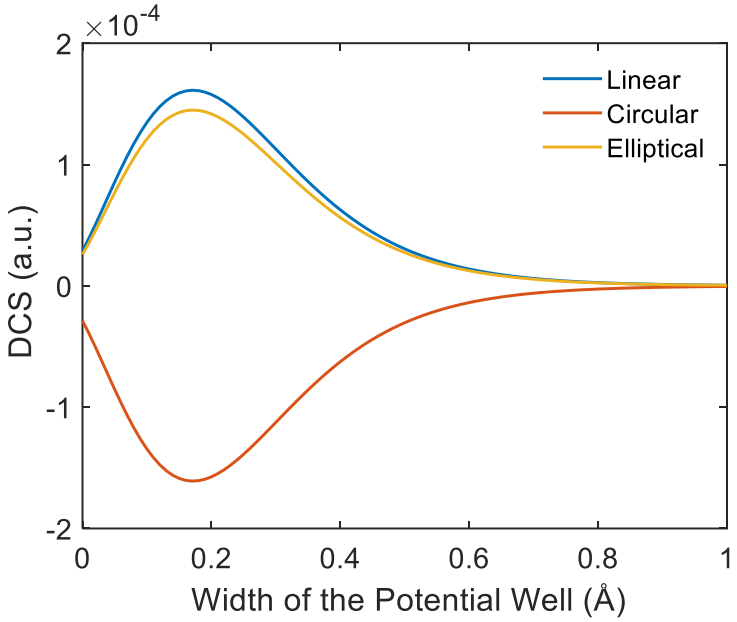

FIGURE 4. DCS with of the potential well for linear, circular and elliptical

The linear and elliptical polarizations provide valuable insights into the scattering behavior with varying potential well widths, with linear polarization showing higher DCS values compared to elliptical polarization. The observed trends underscore the importance of selecting appropriate polarization conditions for accurate and effective analysis of scattering processes. The decrease in DCS for larger potential well widths, influenced by the Bessel function, highlights the complex interplay between potential well width and scattering efficiency.

The study of DCS under different polarization conditions and screening parameters has important practical applications across various fields. In nuclear reactions, particularly within metals, electron screening can be leveraged to enhance reaction cross-sections, essential for low-energy fusion processes. In laser-molecule interactions, optimizing polarization conditions helps improve control over molecular scattering, aiding in techniques like molecular imaging and spectroscopy. This research also provides valuable insights for designing scattering experiments, particularly in particle physics and electron microscopy, where maximizing scattering efficiency is crucial. Additionally, in materials science, understanding the interplay between polarization and screening can guide the development of advanced materials, such as semiconductors and nanotechnology, by improving control over electron behavior.

CONCLUSION

This study reveals that the differential cross section (DCS) for scattering processes varies with polarization conditions (linear, circular, elliptical), screening parameters, potential strength, and potential well width. DCS decreases with increasing screening parameters, with linear and circular polarizations yielding similar values and elliptical polarization showing higher DCS due to stronger interaction effects. The DCS increases with initial momentum, exhibiting fluctuations between 8-11 MeV before stabilizing, with linear polarization providing higher DCS. For potential strength, DCS initially drops but rises beyond 4 eV, with linear polarization being the most effective. As for the potential well width, DCS increases with smaller widths, peaking at 0.14 Å and then decreasing, with linear and elliptical polarizations demonstrating significant changes while circular polarization shows minimal impact. These findings highlight the critical role of polarization and parameter selection in understanding and controlling scattering behaviors.

REFERENCES

[1] A. Jaron-Becker, "Molecular dynamics in strong laser fields," *IEEE Journal of Selected Topics in Quantum Electronics*, vol. 18, no. 1, pp. 105-112, 2011.
[2] S. Varró, S. Hack, G. Paragi, P. Földi, I. F. Barna, and A. Czirják, "Diatomic molecule in a strong infrared laser field: Level-shifts and bond-length change due to laser-dressed Morse potential," *New Journal of Physics*, vol. 25, no. 7, p. 073001, 2023.
[3] M. Wei et al., "Two-center interference effect in ionization of diatomic molecules subject to close-to-circularly-polarized femtosecond laser fields," *Physical Review A*, vol. 98, no. 6, p. 063418, 2018.
[4] P. Stammer et al., "Quantum electrodynamics of intense laser-matter interactions: A tool for quantum state engineering," *PRX Quantum*, vol. 4, no. 1, p. 010201, 2023.
[5] P. B. Corkum, "Plasma perspective on strong field multiphoton ionization," *Physical Review Letters*, vol. 71, no. 13, p. 1994, 1993.
[6] A. Palacios, J. L. Sanz-Vicario, and F. Martín, "Theoretical methods for attosecond electron and nuclear dynamics: Applications to the H_2 molecule," *Journal of Physics B: Atomic, Molecular and Optical Physics*, vol. 48, no. 24, p. 242001, 2015.
[7] Z. Sun and N. Lou, "Autler-Townes splitting in the multiphoton resonance ionization spectrum of molecules produced by ultrashort laser pulses," *Physical Review Letters*, vol. 91, no. 2, p. 023002, 2003.
[8] K. Yadav et al., "Elliptically polarized laser-assisted elastic electron-hydrogen atom collision in Coulomb potential," *Eurasian Physical Technical Journal*, vol. 18, no. 4(38), pp. 82-87, 2021.
[9] S. H. Dhobi et al., "Differential cross-section in the presence of a weak laser field for inelastic scattering," *Ukrainian Journal of Physics*, vol. 67, no. 4, p. 227, 2022.
[10] S. H. Dhobi et al., "Study of thermodynamics of a thermal electron in scattering," *Heliyon*, vol. 8, no. 12, 2022.
[11] S. H. Dhobi et al., "Differential cross section with Volkov-thermal wave function in Coulomb potential," *Atom Indonesia*, vol. 1, no. 1, pp. 19-25, 2024.
[12] D. M. Volkov, "On a class of solutions of the Dirac equation," *Zeitschrift für Physik*, vol. 94, pp. 250-260, 1935.
[13] C. J. Joachain, P. Francken, A. Maquet, P. Martin, and V. Véniard, "(e, 2e) collisions in the presence of a laser field," *Physical Review Letters*, vol. 61, p. 165, 1988.
[14] M. Mohan and P. Chand, "Electron-impact ionization of the hydrogen atom in the presence of an intense laser beam," *Phys. Lett. A*, vol. 65, no. 5-6, pp. 399-401, 1978.
[15] E. Maghsoodi, H. Hassanabadi, and O. Aydoğdu, "Dirac particles in the presence of the Yukawa potential plus a tensor interaction in SUSYQM framework," *Phys. Scr.*, vol. 86, p. 015005, 2012.

[16] M. Zarezadeh and M. K. Tavassoly, "Solution of the Schrodinger equation for a particular form of Morse potential using the Laplace transform," *Chin. Phys. C (HEP & NP)*, vol. 37, p. 043106, 2009.
[17] A. M. Desai, N. Mesquita, and V. Fernandes, "A new modified Morse potential energy function for diatomic molecules," *Phys. Scr*., vol. 95, p. 085401, 2020.
[18] D. A. Morals, "Supersymmetric improvement of the Pekeris approximation for the rotating Morse potential," *Chem. Phys. Lett*., vol. 394, pp. 68-75, 2004.
[19] R. Khordad and A. Ghambari, "Theoretical prediction of thermodynamic functions of TiC: Morse ring-shaped potential," *J. Low Temp. Phys*., vol. 199, pp. 1-13, 2020.
[20] J. Cruz, H. Luís, M. Fonseca, and A. P. Jesus, "Electron screening effects in nuclear reactions: still an unsolved problem," in *Journal of Physics: Conference Series*, vol. 337, no. 1, p. 012062, Feb. 2012, IOP Publishing.
[21] Y. D. Jung and K. S. Lee, "Screening effects on nonrelativistic bremsstrahlung in the scattering of electrons by neutral atoms," *Astrophys. J.*, vol. 440, NASA-TM-112928, 1995.
[22] M. Čalkovský, M. Hugenschmidt, E. Müller, and D. Gerthsen, "Differential Electron Scattering Cross-Section at Low Electron Energies: The Influence of the Screening Parameter," *Microsc. Microanal*., vol. 25, no. S2, pp. 464-465, 2019, doi:10.1017/s1431927619003052.
[23] K. Bartschat, J. Tennyson, and O. Zatsarinny, "Quantum-mechanical calculations of cross sections for electron collisions with atoms and molecules," *Plasma Process. Polym*., vol. 14, no. 1-2, p. 1600093, 2017.
[24] O. Zatsarinny, Y. Wang, and K. Bartschat, "Electron-impact excitation of argon at intermediate energies," *Phys. Rev. A*, vol. 89, no. 2, p. 022706, 2014.
[25] M. Kurokawa et al., "High-resolution total-cross-section measurements for electron scattering from Ar, Kr, and Xe employing a threshold-photoelectron source," *Phys. Rev. A*—At., Mol., Opt. Phys., vol. 84, no. 6, p. 062717, 2011.
[26] V. Zeman, K. Bartschat, C. Norén, and J. W. McConkey, "Near-threshold electron-impact excitation of the vacuum-ultraviolet resonance transitions in Ne, Ar, Kr, and Xe," *Phys. Rev. A*, vol. 58, no. 2, p. 1275, 1998.